





Root uptake dominates mercury accumulation in permafrost plants of Qinghai-Tibet Plateau

Xun Wang ¹, Wei Yuan¹, Che-Jen Lin^{2,3}, Dingyong Wang⁴, Ji Luo⁵, Jicheng Xia ¹, Wei Zhang¹, Feiyue Wang ⁶ & Xinbin Feng ¹✉

Uptake of atmospheric elemental mercury via foliage is thought to be the dominant pathway of mercury accumulation in terrestrial ecosystems, including those in the Arctic permafrost regions. Whether a similar process operates in alpine permafrost regions remains unknown. Here we report mercury concentrations and stable isotopic signatures in a large cluster alpine permafrost regions of mid-latitude Qinghai-Tibet Plateau. We find a transition from foliage to root uptake of mercury as elevation increases. In alpine permafrost regions, we find that root uptake of mercury from the surrounding soil is the dominant accumulation pathway. We estimate that root uptake accounts for $70 \pm 19\%$ of plant mercury in permafrost regions of the Qinghai-Tibet Plateau and propose that this may be related to the harsh climate conditions suppressing foliage growth and promoting lateral root growth.

¹State Key Laboratory of Environmental Geochemistry, Institute of Geochemistry, Chinese Academy of Sciences, Guiyang, China. ²Center for Advances in Water and Air Quality, Lamar University, Beaumont, TX, USA. ³Department of Civil and Environmental Engineering, Lamar University, Beaumont, TX, USA. ⁴College of Resources and Environment, Southwest University, Chongqing, China. ⁵Key Laboratory of Mountain Surface Processes and Ecological Regulation, Institute of Mountain Hazards and Environment, Chinese Academy of Sciences, Chengdu, China. ⁶Centre for Earth Observation Science, and Department of Environment and Geography, University of Manitoba, Winnipeg, MB, Canada. ✉email: fengxinbin@vip.skleg.cn

The 2017 Minamata Convention on Mercury (Hg), a legally binding international treaty, aims to protect human health and the environment from the impact of Hg pollution by curtailing anthropogenic Hg emissions. However, knowledge gaps in global Hg cycling challenge our ability to assess the effectiveness of the Convention in reducing human and wildlife Hg exposure^{1–4}. For example, the fate of the large quantity of Hg stored in the permafrost regions, estimated at 600–1700 Gg in permafrost soil of 0–3 m depth^{5,6}, is poorly constrained. In a warming climate, thawing of permafrost may release this legacy Hg into the atmosphere at a rate that could impact global ecosystems^{5–9}, and possibly offset the emission reduction efforts for anthropogenic Hg. After the Hg release, vegetation succession and biomass growth in the cryosphere promote atmospheric elemental Hg (Hg⁰) uptake and act as an active sink^{10,11}. However, little is known about the cycling of Hg in the alpine permafrost regions outside of the Arctic.

Located at mid-latitude (26–40°N), the Qinghai-Tibet Plateau (QTP) hosts the largest alpine permafrost clusters in the world, covering an area of $\sim 1.2 \times 10^6$ km² and representing $\sim 40\%$ of global alpine permafrost areas^{8,12,13}. The region has experienced accelerated warming, wetting, and thawing over recent decades^{12,14}. Earlier studies have estimated 21.7 Gg of Hg stored in the surface 3-m of permafrost soils in the QTP, which is equivalent to 8% of the permafrost Hg pool in the Northern Hemisphere⁸. Climate-induced landscape perturbations and changes in vegetation and hydrogeochemical processes in the QTP permafrost regions may influence Hg biogeochemical cycling^{6,7,9,15}, and may lead to rapid release of legacy Hg to the atmosphere. Thus, understanding Hg cycling in this alpine permafrost region can help assess the ecological and human health risk caused by Hg in the QTP and downstream regions, as well as the collective impact of thawing permafrost to global Hg cycling in a changing climate.

Earlier studies suggest the importance of root uptake^{16–18} but recent studies confirm that foliage uptake of atmospheric Hg⁰ is actually the dominant uptake pathway of Hg in most above-ground vegetation^{10,11,19–24}, with the exception of selected aquatic vegetation in wetlands^{25,26}. This is because Hg is largely blocked in the root zone by cell wall membranes^{27,28}, resulting in limited root uptake (<10%) and transfer to aboveground biomass²⁵. At elevations of more than 4000 m above sea level, the severe climate (e.g., low air pressure and temperature, strong wind, low precipitation, intense solar ultraviolet (UV)) in the QTP alpine permafrost promotes enhanced root growth and vegetation interaction with thawing permafrost soil^{29,30}. We hypothesize that the combination of geochemical and ecological processes driven by the extreme climatic conditions, such as strong UV irradiance, and high elevation in QTP, promote Hg accumulation pathways in vegetation that differ from those observed in low-land regions.

Characteristics of Hg stable isotopes, including mass-dependent fractionation (MDF; the change of stable isotope composition due to a process of interest depends on the atomic mass of the isotope; reported as $\delta^{202}\text{Hg}$) and mass-independent fractionation (MIF; the change of stable isotope composition due to the process of interest does not scale in proportion to the masses of individual isotopes; reported as $\Delta^{199}\text{Hg}$ and $\Delta^{201}\text{Hg}$ for odd-MIF and $\Delta^{200}\text{Hg}$ for even-MIF), offer new insight in identifying Hg sources and understanding accumulation processes in the ecosystems. Hg from atmospheric deposition and geogenic sources displays distinctly unique Hg isotopic signatures. Biogeochemical processes of Hg in the environment also exhibit unique isotopic fractionations^{10,11,19–24}. The primary cause of MIF of Hg is the photochemical reduction of Hg(II) species, and the magnitude of this MIF of Hg depends on the complexing

ligand and reaction conditions. For example, during photo-reduction of Hg(II) by low-molecular-weight organic compounds, S-containing ligands promote preferential enrichment of ¹⁹⁹Hg and ²⁰¹Hg in the product of Hg⁰, while ligands without sulfur promote enrichment of ¹⁹⁹Hg and ²⁰¹Hg in the reactant (Hg(II))^{31–33}.

Here we report the isotopic distribution of Hg in seasonally frozen-soil and permafrost regions of the QTP to quantify the sources, accumulation, and post-depositional processes of Hg in vegetation and soils. The study was conducted at the permafrost and seasonally frozen ground sites of the Sanjiangyuan (Three-River Headwaters) National Nature Reserve and the Nu River Headwaters Region. The region covers more than 2000 m elevation difference over $\sim 5.0 \times 10^5$ km² area (Supplementary Fig. 1a–c). Known as the “Asian Water Tower”, it is the origin of major river systems of the world. The vegetation cover is mainly alpine meadow and steppe, whose distributions vary with local climatic conditions and biological adaptability. Twenty-one sites were studied in June 2020, including 13 in alpine meadows and 8 in alpine steppes. Four sites (S01, S11, S19, and S21) have seasonally frozen soil ground, and 17 sites have permafrost cover (Fig. 1a and Supplementary Fig. 1). We determined the Hg concentration and isotopic signatures of grass foliage, root, rhizospheric soils, surface soils (0–17 cm depth herein), deep soils (more than 25 cm depth herein), and bedrock; then assessed the Hg spatial distribution and accumulation sources in vegetation and soils by Hg isotopic mixing models.

Results and discussion

Spatial distribution of Hg signatures. Grass root has the highest observed Hg concentration while bedrock has the lowest ($p < 0.05$, by One-Way ANOVA test, Fig. 1b). The measured Hg concentrations in grass foliage were comparable to those found in foliage of steppes and meadows ($p = 0.65$ by Kruskal-Wallis test, Supplementary Fig. 2), suggesting grass type is not the main factor influencing variations in foliar Hg concentration. The Hg concentration and pool size in grass foliage did not differ significantly between the permafrost and seasonally frozen ground regions (all $p > 0.05$ by Kruskal-Wallis test), while the average Hg concentration and pool size in the surface soil of frozen ground regions were 35–45% higher than in soil of permafrost (Supplementary Fig. 3). The highest $\delta^{202}\text{Hg}$ signatures were measured in the bedrock at $-0.23 \pm 0.50\text{‰}$, while the lowest values of $-1.49 \pm 0.59\text{‰}$ were measured in the grass foliage ($p < 0.05$ by Kruskal-Wallis test). Similar values in the range of -0.67‰ to -0.85‰ were found in the rhizospheric and surface soil (Fig. 1c). Except for the significantly lower $\Delta^{199}\text{Hg}$ in the bedrock at $-0.06 \pm 0.04\text{‰}$ ($p < 0.05$ by Kruskal-Wallis test), most $\Delta^{199}\text{Hg}$ signatures were similar in vegetation biomass and surface soils (Fig. 1d). The $\Delta^{200}\text{Hg}$ signatures were close to zero for all samples (Fig. 1e), and the 0–5 cm depth and rhizospheric soils had the lowest values ($p < 0.05$ by Kruskal-Wallis test).

Hg concentration in foliage did not vary significantly with latitude (Supplementary Fig. 4a). The foliar Hg pool, surface soil Hg concentration and surface soil Hg pool size all decreased with latitude. The $\Delta^{199}\text{Hg}$ in surface soil increased with latitude (Supplementary Fig. 4b, c; Fig. 2a, b). The significant correlation between precipitation intensity and surface soil Hg concentrations (Fig. 2c) and pool size (Fig. 2d) suggests that rainfall influences the spatial distribution of atmospheric Hg deposition. Higher precipitation at lower latitude (Supplementary Fig. 1) may increase atmospheric Hg²⁺ deposition and enhance atmospheric Hg⁰ uptake by vegetation through greater biomass production. The effect of precipitation in promoting vegetation growth is

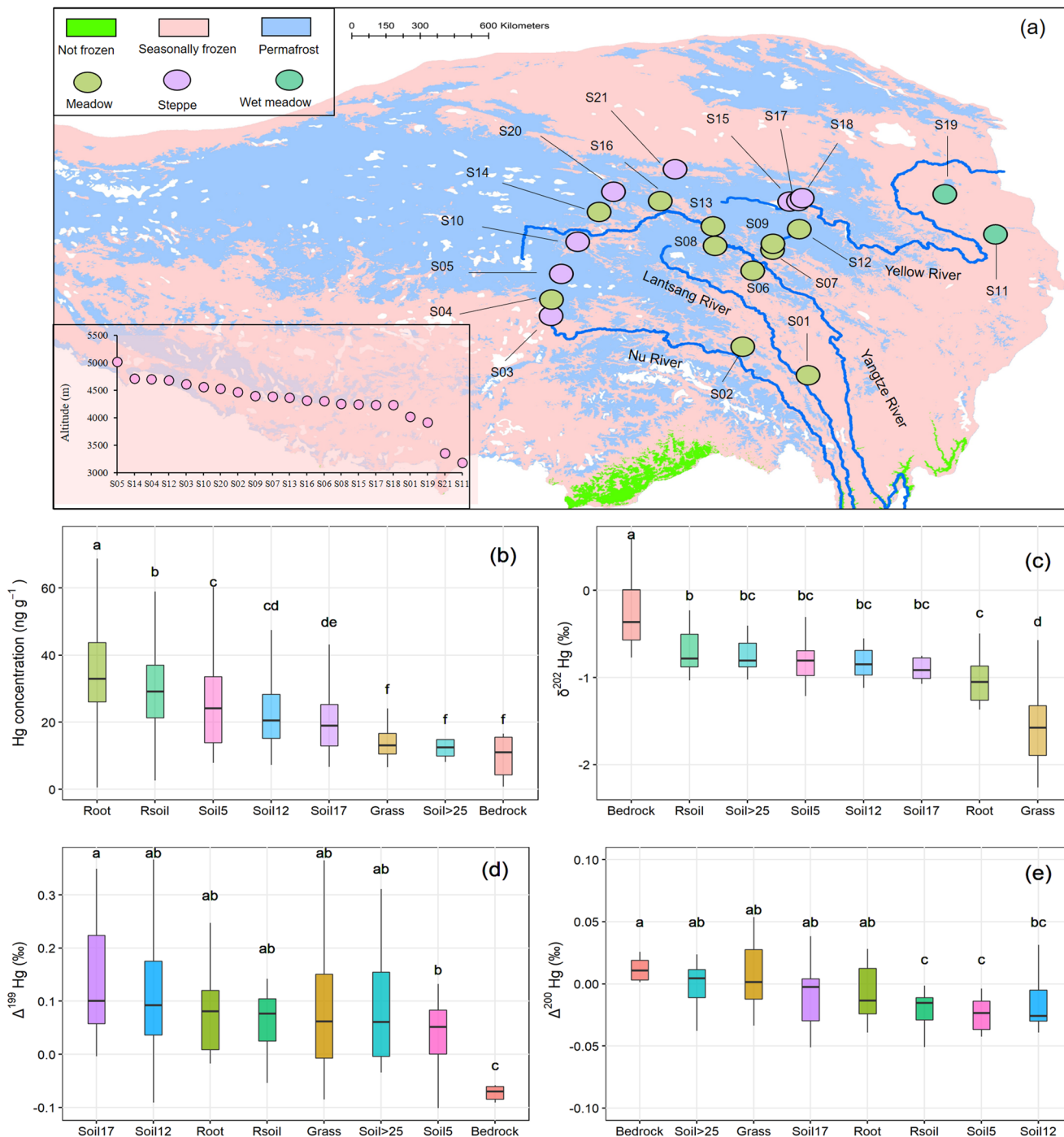


Fig. 1 Spatial distribution of mercury (Hg) concentration and isotopic composition in grass foliage, roots, and soil layers. **a** Site location, **b** Hg concentration, **c** $\delta^{202}\text{Hg}$ (‰), **d** $\Delta^{199}\text{Hg}$ (‰), **e** $\Delta^{200}\text{Hg}$ (‰). The permafrost distribution in **a** is from the earlier study⁷⁶. The term Rsoil means rhizosphere soil, and Soil5 is 0–5 cm depth soil, and Soil12 is 5–12 cm depth soil, and Soil17 is 12–17 cm depth soil, and Soil > 25 is the soil more than 25 cm depth. Boxplot elements in **b–e** show the median (midline), the interquartile range of 25% and 75% percentile (box boundaries), data points within the 1.5 × quartile range (whiskers). The letter in **b, e** donates the statistical difference at the 95% confidence level.

clearly shown in Supplementary Fig. 5a. The soil organic matter (SOC) in the surface soil comes from decomposition of litter, with a higher soil SOC content acting to lower soil pH³⁴. The significant correlation between soil Hg concentration and SOC (Supplementary Fig. 5b), anticorrelation between soil Hg concentration and pH (Supplementary Fig. 5c), and correlation between aboveground grass biomass and soil Hg pool sizes (Supplementary Fig. 5d) all indicate an important role of vegetation in promoting Hg accumulation in soils. In addition,

the greater SOC produced by vegetative biomass likely also retains a larger amount of Hg in soil through processes such as complexation^{19,20}. The $\Delta^{199}\text{Hg}$ values of vegetative biomass (Fig. 2e) and surface soil (Fig. 2f) both increase with altitude. Given the reduced air pressure, lower temperature, higher UV irradiance and stronger winds at elevated altitude³⁵, these correlations suggest that the change of climatic and environmental conditions along with altitude may influence the Hg accumulation in vegetation and soils.

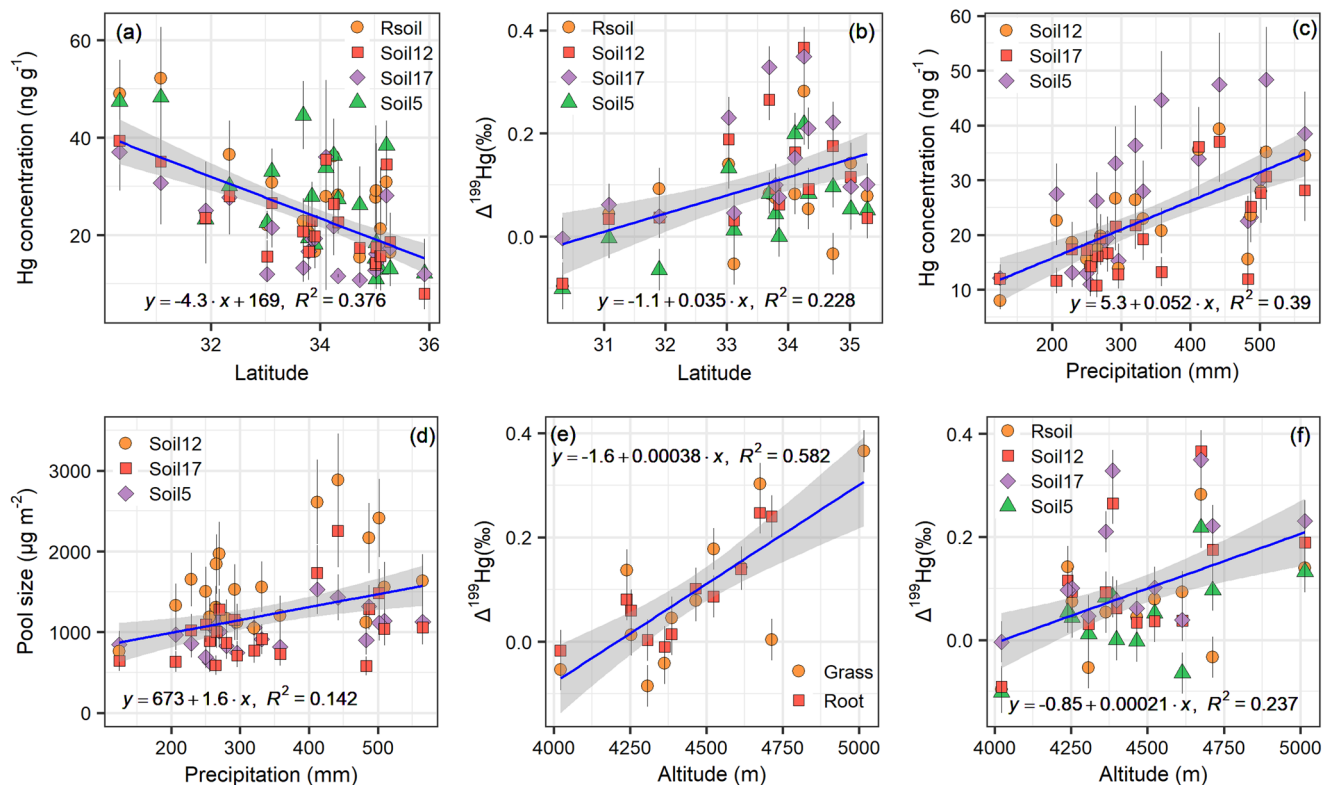


Fig. 2 Relationship between mercury (Hg) concentration and latitude, precipitation, and altitude. **a** Correlations for Hg concentration versus latitude, **b** $\Delta^{199}\text{Hg}$ in soils versus latitude, **c** precipitation versus Hg concentration in soils, **d** precipitation versus pool size in soils, **e** $\Delta^{199}\text{Hg}$ in vegetation versus altitude, **f** $\Delta^{199}\text{Hg}$ in surface soils versus altitude. The shading of **a–f** represents the 95% confidence interval for regression and error bars stand for 1σ .

Mercury accumulation in vegetation. Since Hg uptake by vegetation causes little Hg-MIF^{19,36}, the Hg-MIF is a useful tracing tool for identifying Hg sources in vegetation. The atmospheric Hg^0 exhibits negative $\Delta^{199}\text{Hg}$ and $\Delta^{200}\text{Hg}$ signals, while atmospheric Hg^{2+} has the distinctly positive $\Delta^{199}\text{Hg}$ and $\Delta^{200}\text{Hg}$ signals. The reported $\Delta^{199}\text{Hg}$ signatures in foliage of low-altitude ecosystems across the globe are $-0.25 \pm 0.18\text{‰}$, similar to those of atmospheric Hg^0 because of foliage uptake^{11,19,22,37,38}. The observed $\Delta^{199}\text{Hg}$ values in grass foliage at high altitude are significantly different from those recorded in low-altitude terrestrial ecosystems (Figs. 1d and 3a), with $\Delta^{199}\text{Hg}$ in grass foliage showing a positive shift of 0.2‰ to 0.4‰ compared to the signals found in foliage of low-altitude regions. These data suggest that atmospheric Hg^0 uptake is not an important pathway for foliage Hg uptake in the QTP region.

The atmospheric Hg^{2+} at the study sites has higher $\Delta^{199}\text{Hg}$ values of $0.89 \pm 0.18\text{‰}$ (Supplementary Table 1) compared to the global average of $0.54 \pm 0.30\text{‰}$ ^{19,20}, uncharacteristic of elevated terrains with little influence from direct anthropogenic emissions. This led us to examine the influence of deposited atmospheric Hg^{2+} to the cuticle of foliage, which might contribute to the positive $\Delta^{199}\text{Hg}$ signatures in foliage. $\Delta^{200}\text{Hg}$ shifts are caused by photo-oxidation in the troposphere and relatively insensitive to other Hg biogeochemical processes^{36,39}, thus useful to identify Hg sources that are of atmospheric Hg^{2+} origin. The much smaller $\Delta^{200}\text{Hg}$ values in the foliage than those found in precipitation suggest that the contribution from atmospheric Hg^{2+} deposition was negligible (Fig. 3b).

The strong correlation in odd-MIF signatures among foliage, root, and rhizospheric soil (Supplementary Table 2) suggests that root uptake of soil Hg might be an important pathway for Hg accumulation in foliage. Furthermore, $\Delta^{199}\text{Hg}$ and $\delta^{202}\text{Hg}$ of grass foliage show the following relationship with Hg

concentration (Fig. 3c, d) except at Site 11, a wet meadow with positive $\Delta^{199}\text{Hg}$ values likely influenced by the meltwater Hg inputs having positive $\Delta^{199}\text{Hg}$:²²

$$\Delta^{199}\text{Hg} = 0.02 \pm 0.01 \times \text{Hg} - 0.20 \pm 0.10\text{‰}, R^2 = 0.53 \quad (1)$$

$$\delta^{202}\text{Hg} = 0.07 \pm 0.01 \times \text{Hg} - 2.45 \pm 0.17\text{‰}, R^2 = 0.80 \quad (2)$$

Extrapolating this relationship to a zero Hg concentration using Eq. (1) results in a $\Delta^{199}\text{Hg}$ value of $-0.20 \pm 0.10\text{‰}$, approaching $\Delta^{199}\text{Hg}$ values commonly found for atmospheric Hg^0 in remote regions of QTP ($-0.20 \pm 0.07\text{‰}$, Supplementary Table 3)⁴⁰. The intercept of Eq. (2) is consistent with the known MDF for foliage uptake of atmospheric Hg^0 , which has a global median MDF value of -2.80‰ ^{11,19,22,37,38}. Lower Hg concentrations in roots and foliage were found at lower elevations at Site 06 and 01 (Supplementary Fig. 1d), with up to -0.08 to -0.05‰ of $\Delta^{199}\text{Hg}$, which were close to the signatures of atmospheric Hg^0 . The highest $\Delta^{199}\text{Hg}$ of 0.37‰ was found at Site 05, a permafrost site at 5000 m above sea level (Supplementary Fig. 1d). Finally, the geochemical indicator of Ti (Titanium, more discussion in Supplementary Note 1), which is mainly found in root due to uptake from surrounding soils^{41–43}, also supports the hypothesis of root Hg uptake due to a strong positive correlation of Hg and Ti in root and a weak negative correlation in soils (Supplementary Fig. 6).

Given the 0.3–0.6‰ shift of $\Delta^{199}\text{Hg}$ and comparable $\Delta^{200}\text{Hg}$ between endmembers of atmospheric Hg^0 and surface soil Hg, the signal of $\Delta^{199}\text{Hg}$ is a better tracer than $\Delta^{200}\text{Hg}$ for determining Hg sources in grass vegetation. The $\Delta^{199}\text{Hg}$ mixing model (Fig. 4a) shows that the contribution of Hg derived from soil surrounding roots is similar to that in foliage ($67 \pm 21\%$ versus $70 \pm 19\%$). Our findings suggest that $\sim 70\%$ Hg in foliage

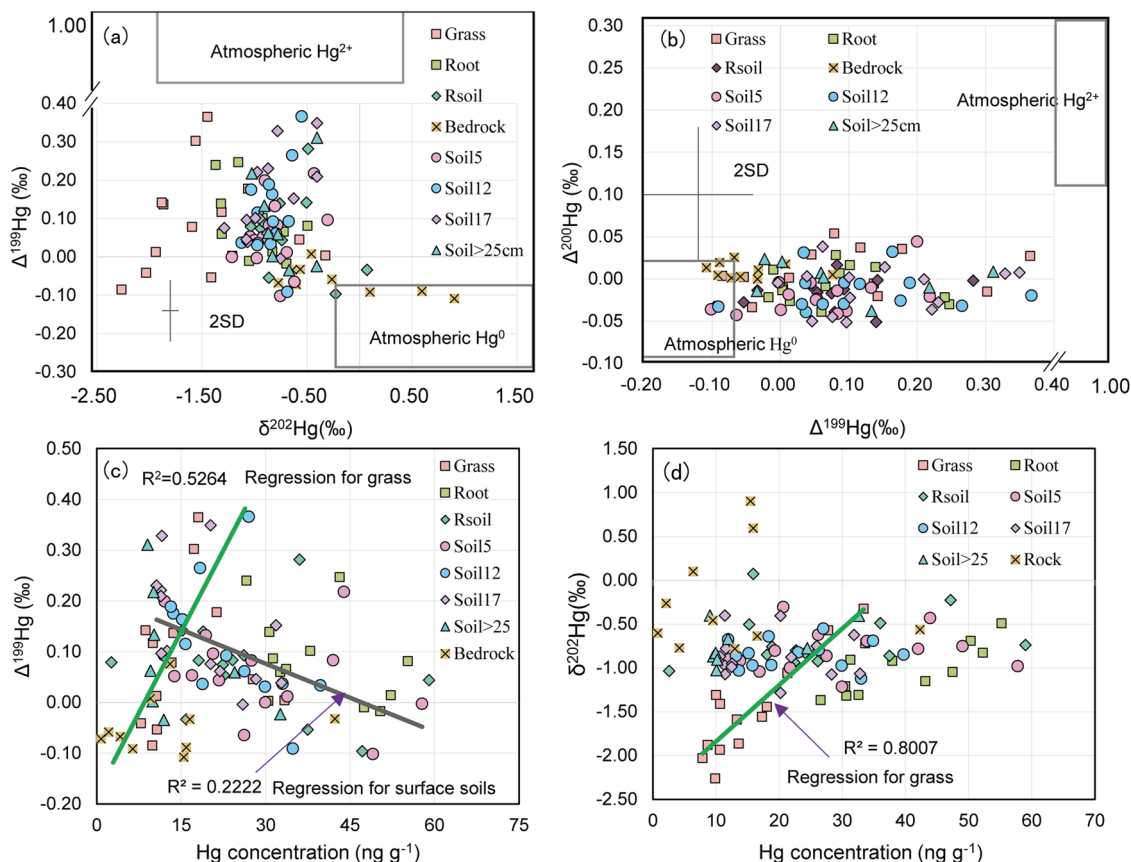


Fig. 3 Relationships between different mercury (Hg) and isotopic compositions. **a** $\Delta^{199}\text{Hg}$ versus $\delta^{202}\text{Hg}$, **b** $\Delta^{200}\text{Hg}$ versus $\Delta^{199}\text{Hg}$, **c** $\Delta^{199}\text{Hg}$ versus Hg concentration, **d** $\delta^{202}\text{Hg}$ versus Hg concentration. Two standard deviations are shown in **a** and **b**. The green line in **c** represents the regression between $\Delta^{199}\text{Hg}$ and Hg concentration for grass foliage samples, and gray line represents the regression between $\Delta^{199}\text{Hg}$ and Hg concentration for 0–17 cm depth of surface samples. The green line in **d** represents the regression between $\delta^{202}\text{Hg}$ and Hg concentration for grass foliage samples. The atmospheric Hg^{2+} isotopic compositions in the QTP can be found in Supplementary Table 1, and the range of atmospheric Hg^0 isotopic composition is based on literature synthesis^{19,40} and for the QTP region can be found in Supplementary Table 3.

on the QTP is derived from soil-root-foliage transport, and ~30% Hg in vegetation from atmospheric Hg^0 uptake.

The relatively large difference between ~0.00‰ of $\Delta^{200}\text{Hg}$ in roots and 0.25 ± 0.19 ‰ in precipitation (Fig. 3b) suggests that wet Hg^{2+} deposition is not the main source of Hg^{2+} to soils. Available Hg for root uptake could be from desorption of soil Hg and therefore exhibits similar isotopic compositions as soil. We found that the contribution of root uptake of soil Hg increased with altitude (Fig. 4b), leading to more positive $\Delta^{199}\text{Hg}$ signals in vegetative biomass at higher elevation as demonstrated by the increase in $\Delta^{199}\text{Hg}$ in grass foliage and roots with altitude (Fig. 2e).

Atmospheric Hg^0 uptake by foliage has been regarded as the dominant Hg source in vegetation in low-altitude ecosystems, but our data indicate that this is not the case in the QTP permafrost region^{10,11,19–24}. The physiological mechanism underlying enhanced root uptake of soil Hg in elevated permafrost regions needs further study. A plausible explanation may be that the low temperature and air pressure, strong UV irradiance and dry air at high altitude impose stress and force vegetation to capture water and nutrients from thawing permafrost soil through root uptake for survival^{29,30}, thus facilitating a greater soil Hg uptake by root. This can be partly supported by the vegetation morphologic and metabolic changes to adapt to the harsh climatic and environmental conditions in elevated regions. For example, the harsh climate suppresses foliage growth, but promotes lateral root growth and enhances the production of root exudate^{44–47}.

These vegetation morphologic and metabolic changes are beneficial for soil Hg uptake by root. The relatively stronger UV irradiance in the alpine permafrost region can distinctly reduce respiration and photosynthesis, which limits atmospheric Hg^0 uptake by foliage^{44–47}, in addition to enhancing Hg photo-reduction and volatilization from plant surfaces⁴⁸. Additionally, since foliage uptake of air Hg^0 progresses as a first-order process depending on the air Hg^0 concentration^{19,49}, a lower flux of foliage Hg^0 uptake is expected given the lower mass concentration of Hg^0 in the ambient air of QTP. Finally, different grass species may respond to the climatic and environmental conditions in the QTP at various degrees, and therefore the grass species may also influence the atmospheric Hg^0 uptake. With the sampling methodology in this study, the impact caused by grass species could not be discerned. It is therefore possible that the difference in grass species could have introduced noises to the isotope signatures that did not follow the overall trend with elevations.

Hg accumulation in surface soil. The similarity in Hg MIF characteristics in soil among 0–5 cm, 5–12 cm, and 12–17 cm depth suggest similar Hg biogeochemical processes in the uppermost surface soil (Fig. 1d, e). Three source endmembers have been identified for soil Hg, including atmospheric Hg^0 uptake, atmospheric Hg^{2+} deposition and geogenic sources (i.e., weathering processes induced rock Hg release into soils)^{10,19,22,23,50,51}. The strong UV radiation in the QTP may

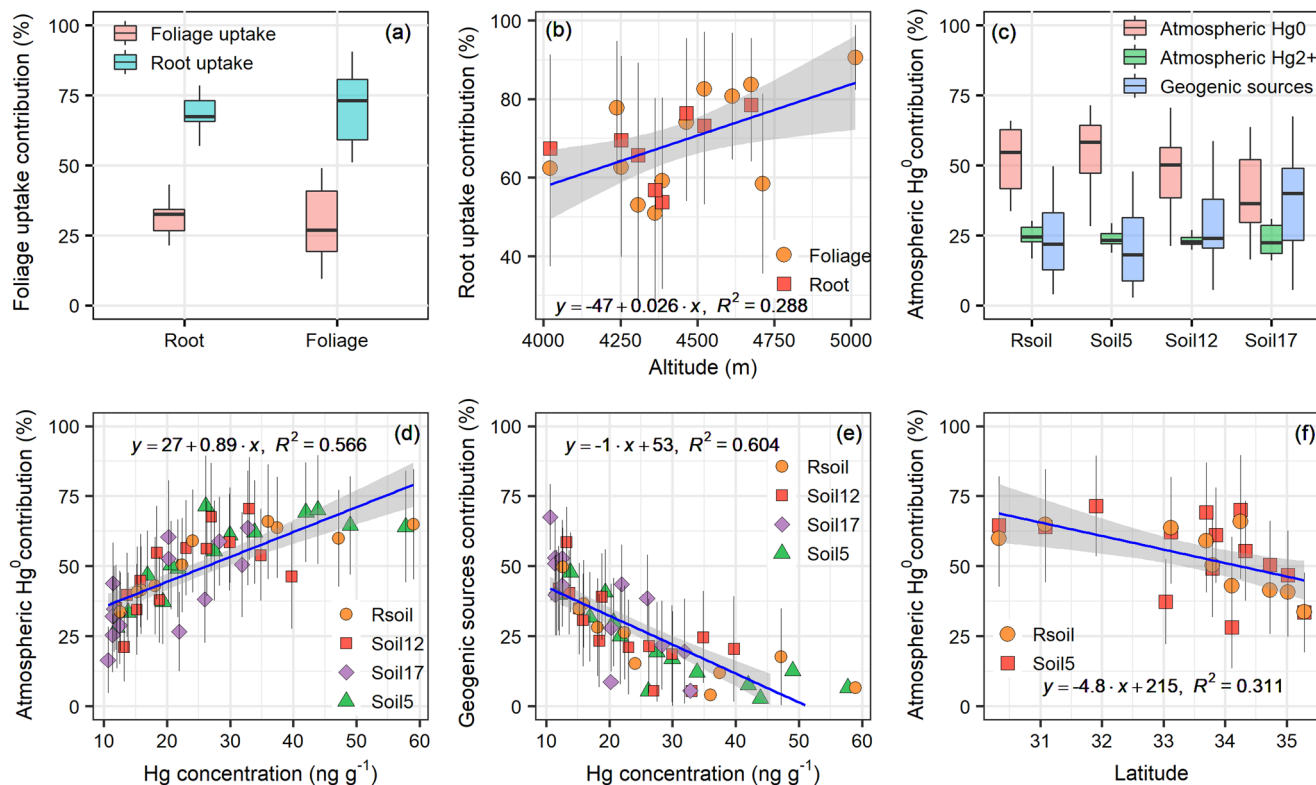


Fig. 4 Summary of estimates from the mercury (Hg) isotopic and source attribution model. **a** Source attribution using the Hg isotopic model for vegetation, **b** correlation for contribution of root uptake of soil Hg in vegetation versus altitude, **c** source attribution using the Hg isotopic model for soils, **d** correlation for soil Hg concentration versus foliage uptake of atmospheric Hg⁰ sources in surface soil, **e** correlation for contribution of geogenic sources versus Hg concentration, **f** correlation for latitude versus foliage uptake of atmospheric Hg⁰ sources. All regressions reach the significant level at the 95% confidence. Boxplot elements in **a** and **c** show the median (midline), the interquartile range of 25% and 75% percentile (box boundaries), data points within the 1.5 × quartile range (whiskers). The shading in **b, d–f** represents the 95% confidence interval for regression, and error bars stand for 1 σ .

enhance photo-reduction in surface soil to induce a shift of odd-MIF, but without an even-MIF. Therefore, the $\Delta^{200}\text{Hg}$ signatures in soil is a superior tracer to identify the Hg sources. Ti is selected as a tracing element for geogenic sources since it is conserved in chemical weathering processes⁵². Using Hg/Ti ratios and $\Delta^{200}\text{Hg}$ signatures, the source contribution of Hg in the uppermost soil profiles includes 40–55% from atmospheric Hg⁰ deposition, 23–25% from precipitation Hg²⁺ and 23–38% from geogenic sources (Fig. 4c). The contribution of atmospheric Hg⁰ deposition decreases with soil depth with increasing contribution of geogenic sources (Fig. 4c).

The $\Delta^{199}\text{Hg}$ in soil Hg decreases with increasing soil Hg concentration (Fig. 3c), which we attribute to a greater contribution from foliage uptake of atmospheric Hg⁰ (Fig. 4d) and smaller geogenic source contribution (Fig. 4e) at elevated sites. Latitude anticorrelates with atmospheric Hg⁰ contribution (Fig. 4f), confirming that higher vegetation biomass in lower latitude can increase the atmospheric Hg⁰ uptake. The estimated fraction of atmospheric Hg²⁺ input justifies the 0.08–0.20‰ value of $\Delta^{199}\text{Hg}$ found in soil. However, this cannot explain the odd-MIF of soil Hg increasing with elevation (Fig. 2f) since no gradient trends are observed for the estimated fraction of atmospheric Hg²⁺ input. This is likely caused by post-depositional redox processes⁵⁰.

The slope of $\Delta^{199}\text{Hg}/\Delta^{201}\text{Hg}$ has been used as a diagnostic index to reflect post-depositional redox processes in the environment since the Hg photolytically and organic-matter mediated reactions yield unique slopes of $\Delta^{199}\text{Hg}/\Delta^{201}\text{Hg}$. Photochemical reduction of Hg²⁺ complexed to organic ligands induces positive MIF in the residual Hg²⁺ with a slope of 0.9–1.4

depending on reaction conditions (e.g., pH, dissolved oxygen and the type of organic ligands)^{32,33}. Organic-matter-mediated dark redox induces a slope of 1.6 with the enrichment of odd isotopes in the reactions^{53,54}. Photo-reduction of MeHg is known to cause a positive MIF with a slope of $\Delta^{199}\text{Hg}/\Delta^{201}\text{Hg}$ of 1.6^{36,55}.

The slope of 1.3 for soil $\Delta^{199}\text{Hg}/\Delta^{201}\text{Hg}$ (Fig. 5a) compared to 1.0 for atmospheric Hg²⁺ and Hg⁰ depositions across the globe^{10,19,22,23,50,51}, indicates that post-depositional redox processes induce a positive odd-MIF shift in surface soils. However, the <2% MeHg to total Hg ratio and the weak correlation to $\delta^{202}\text{Hg}$ and $\Delta^{199}\text{Hg}$ (Supplementary Fig. 7) suggest that the transformation between total Hg and MeHg does not support this pathway being responsible for the distinct odd-MIF in the QTP. Flux measurements of 2–25 ng m⁻² h⁻¹ over permafrost soil at Site 05 and Site 14 suggest that solar irradiance enhances soil Hg⁰ evasion^{15,56,57}. Although the Hg isotopic signatures were not quantified in the soil–air Hg⁰ flux in the QTP, controlled experiments indicate that strong UV and enrichment of organic carbon in the uppermost soils could facilitate Hg(II) reduction in the presence of organic ligands and secondary photolysis, which may induce a positive odd-MIF shift and slope of 1.3 in this study^{32,33,54}.

Comparison to observations in Arctic tundra. The Arctic tundra is underlain by permafrost. Earlier studies have reported the Hg distribution and sources in the vegetation and soil, specifically in Alaska and Siberia^{5,6,10,11,58}. The Arctic tundra regions experience similar low ambient temperatures (annually average < 0 °C) and precipitation (annually average < 400 mm) as in

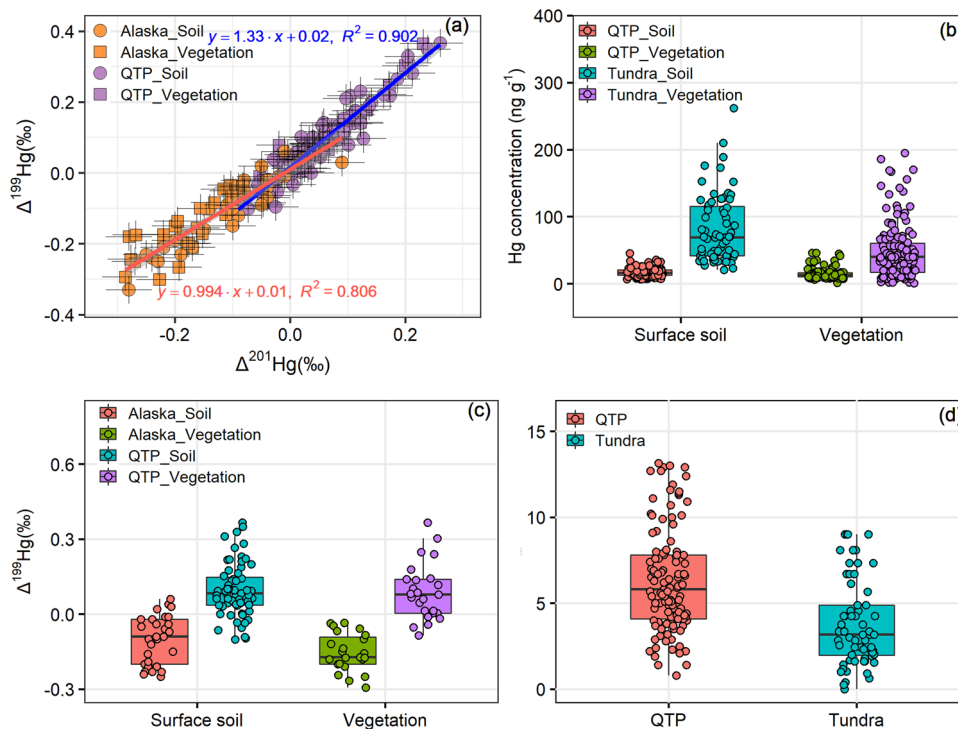


Fig. 5 Variation in mercury (Hg) isotopic composition across soil, vegetation, and region. **a** Comparison of slope for $\Delta^{199}\text{Hg}$ versus $\Delta^{201}\text{Hg}$, **b** Hg concentrations, **c** $\Delta^{199}\text{Hg}$ values in vegetation and 0–30 cm depth surface soils, **d** biomass ratio of root to shoot between the permafrost of QTP and Arctic tundra. Data of Hg concentration and isotopic compositions of Arctic tundra are based on literature synthesis^{5,6,10,11,58}, including the regions of Alaska and Siberia, and the ratio of root to shoot for the grass species in the QTP and tundra are both from earlier studies^{60–62}. Error bars stand for 1σ in **a**. Boxplot elements in **b–d** show the median (midline), the interquartile range of 25% and 75% percentile (box boundaries), data points within the $1.5 \times$ quartile range (whiskers).

the QTP. In contrast, the QTP alpine permafrost regions have more severe climate, e.g., low air pressure, strong wind and intense solar UV, due to its elevation of over 4000 m above sea level. We compared our results to the reported data in the Arctic tundra regions to display the difference of Hg accumulation pathways between the alpine permafrost and Arctic permafrost regions.

The observed slope of $\Delta^{199}\text{Hg}/\Delta^{201}\text{Hg}$ of vegetation and soil samples in Alaska tundra regions is ~ 1.0 (Fig. 5a), which is different to the value of 1.3 found in this study. This suggests that the post-depositional processes in the QTP under high UV radiation (Supplementary Fig. 8) and low air pressure lead to the unique Hg reduction that has not been observed elsewhere in the Arctic tundra^{31,32}. The significantly lower Hg concentration (Fig. 5b, $p < 0.001$, Independent Samples T-test) found in the vegetation and surface soil samples can be attributed to the different vegetation species in the QTP (alpine grass species, e.g., *Kobresia myosuroides*) and in the Arctic tundra (tussock grass, ericaceous shrubs, moss and lichen). Without a root and cuticle layer system, moss and lichen cell walls are easily accessible for atmospheric Hg to be absorbed over the entire surface during the lifespan^{21,59}, leading to elevated Hg concentrations. A much smaller aboveground vegetation Hg pool in the QTP permafrost ($3.3 \pm 1.6 \mu\text{g m}^{-2}$, Supplementary Fig. 2) compared to the value of $29 \mu\text{g m}^{-2}$ in Alaska tundra¹¹ also explains the significantly lower soil Hg concentration in the permafrost regions of QTP.

Biomass and soil samples in the Arctic tundra regions exhibit distinctly negative $\Delta^{199}\text{Hg}$ signatures (Fig. 5c), but air samples show similar MIF characteristics. This suggests foliage uptake of atmospheric Hg^0 being the predominant source^{10,11}. Combining vegetation and soil Hg sources of this study, we estimate that $30 \pm 19\%$ Hg in foliage is from foliage uptake of atmospheric Hg^0 ,

$31 \pm 17\%$ from root uptake of previously deposited Hg^0 , $16 \pm 15\%$ from root uptake of previously deposited Hg^{2+} , and $23 \pm 20\%$ from root uptake of previously geogenic Hg (more details for this calculation can be found in Materials and Methods). This may be due to strong UV and low air pressure in the permafrost regions of QTP forcing morphologic changes of vascular vegetation to adapt the extreme environmental conditions (e.g., root-to-shoot biomass ratio, R/S), leading to a change of Hg accumulation pathway in vegetation^{45,46}. The R/S ratios of grassy species in the QTP permafrost regions nearly double the values found in the Arctic tundra regions (Fig. 5d, $p < 0.001$, Independent Samples T-test). A higher R/S ratio promotes nutrient uptake from soils^{60–62}, thus enhancing root Hg uptake and translocation to foliage.

We recognize that uncertainty exists due to spatio-temporal variability and limited datasets. However, the data are indicative of Hg accumulation processes in the Arctic regions. Both foliage and root uptake pathways may exist simultaneously, but might differ in strength from place to place.

Conclusions and implications

Our study suggests that vegetation adapts to the extreme environmental conditions in the alpine permafrost regions of the QTP, resulting in enhanced root uptake of Hg from surrounding soil and subsequent Hg translocation from root to foliage. Our findings indicate a process that counters the previously reported Hg accumulation pathways in the vegetation of low-altitude ecosystems. While both pathways exist, the contribution from foliage and root uptake by vegetation can be shaped by the environmental conditions.

Recent studies have revealed that the thawing of permafrost has stimulated vegetation productivity in recent decades in the QTP

regions^{12,14}. Therefore, an increase in atmospheric Hg⁰ deposition through vegetative uptake into these permafrost regions can be expected^{20,63,64}. Assuming that weakened atmospheric Hg⁰ uptake by vegetation occurs in the 3.5 million km² of global alpine permafrost regions (20–30% of total permafrost regions in the Northern Hemisphere)¹³, we estimate 6–17 Mg Hg distributed in vegetation of global alpine permafrost regions¹³ using the mean vegetation Hg pool size in this study. Given the 1-year lifespan of grass foliage in permafrost, this represents 2–5 Mg yr⁻¹ of atmospheric Hg⁰ sink caused by foliage uptake, ~70% lower than the estimate using models that assume foliage Hg is derived from atmospheric Hg⁰.

Materials and methods

Site descriptions. Our study regions are located in Sichuan, Qinghai and Tibet provinces (91.6°E–102.8°E, 30.0°N–35.9°N, with an area of about 5.0 × 10⁵ km²), including the Sanjiangyuan (Three-River Headwaters) National Nature Reserve (the headwaters of the Huanghe (Yellow River), Changjiang (Yangtze River) and Lancanjiang-Mekong River, with an area of 3.0 × 10⁵ km²) and the headwater region of the Nuijiang-Salween River (Supplementary Fig. 1). The study sites range in elevation from 3100 m to 5000 m above the sea level. The vegetation cover of these regions is mainly alpine meadow and steppe, which are distributed in different elevations due to the local climatic conditions and biological adaptability. The dominant grass species are *Kobresia myosuroides* (Villars) Foiri, *Leontopodium leontopodioides* (Willd.) Beauv, and *Stipa capillata* L. in alpine steppe, and *Kobresia humilis* Sergievskay, *Poa pratensis* L. and *Stipa capillata* L. in alpine meadow. Specifically, *Kobresia humilis* and *Leontopodium nanum* are dominated in the elevated regions. The soil pH ranges from 5.6 to 9.8 depending on the site locations. The climate is mainly controlled by the Indian and East Asian monsoon in the summer and the Westerlies in the winter⁶⁵. The annual average temperature ranges from -1 °C to 1 °C, and annual precipitation from 400 mm to 600 mm in the seasonally frozen regions, and 200 mm to 400 mm in the permafrost regions. Data of annually precipitation for 2016 in the TGR are obtained from National Tibetan Plateau/Third Pole Environment Data Center (<https://data.tpdc.ac.cn/en/data/3fc66dcd-5db9-4af4-bfc6-55671875a400/>).

Sample collections and measurements. Twenty-one sites were studied in June 2020. The distance between each site ranges from 20 to 350 km. The sampling site is chosen based on the criteria that there is at least 150 m of flat or nearly flat land in the surrounding area and that there are no distinct human activities except for slight livestock grazing in some of the meadows. The sampling locations were identified by global positioning system. At each sampling site, we drew six 5 m × 5 m sampling subplots, and collected samples of the uppermost layers of soils at a depth interval of 0–5 cm, 5–12 cm, and 12–17 cm, deep subsoils (from > 25 cm up to 100 cm depth, depending on the nature of the sites) and bedrocks. We also harvested the aboveground biomass of grass (referred to as grass foliage herein) and grass root from a 50 cm × 50 cm quadrat within a 10-cm depth in each sampling plot, and collected the rhizospheric soil samples from the surface of the grass root for analysis. All samples were put into clean polyethylene bags and stored immediately in a 4 °C portable refrigerator. In total, 200 vegetation and 480 soil samples were collected.

We sampled the precipitation and snow samples at the Sanjiangyuan Alpine Steppe Ecosystem Research Station (SJY, 34°22'N, 100°30'E) in 2021. The sampling methodologies and QA/QC for precipitation and snow are similar to the description in our earlier studies^{20,21}. Briefly, 5 L of water was collected by a precipitation collector. Approximately 5 mL of BrCl and 200 μL SnCl₂ were successively added into the water samples to purge and trap the generated Hg⁰ into the 1 g chlorinate carbon trap. This approach can releases 95 ± 7% of Hg from water samples.

Mercury concentrations in vegetation and soil samples were measured on a DMA80 Hg analyzer, following the protocol described in our earlier studies^{21,66}. Briefly, the National Standard Reference Materials of China GBW07405 (GSS-5, soil, Hg = 290 ± 40 ng g⁻¹), GBW10020 (GSB-11, vegetation, Hg = 150 ± 25 ng g⁻¹) and GBW10049 (GSB-27, vegetation, Hg = 12 ± 3 ng g⁻¹) were used for QA/QC and measured after every 9 samples with a recovery of 95–105%. Soil organic carbon (SOC) content was determined by the Walkley-Back method which involves oxidation of SOC by Cr₂O₇²⁻ followed by the addition of FeSO₄ to reduce the excess Cr₂O₇²⁻⁶⁷. The concentration of titanium (Ti) in vegetation, soil and rock samples was analyzed by Inductively Coupled Plasma Optical Emission Spectroscopy (ICP-OES), following U.S. EPA Method 6020B. Briefly, about 0.1 g soil sample were digested in a closed Teflon vessel by an acid mixture (HNO₃:HF = 5:1, v/v) at 150 °C for 48 hours. The digested solution was transferred quantitatively with ultra-pure water to a 50 mL Teflon bottle and analyzed by ICP-OES (Inductively Coupled Plasma Optical Emission Spectrometer). The SRM, blank and replicated samples were analyzed in every 10 treatments (7 samples + 1 SRM + 1 blank + 1 replicated sample). The average percentages of Ti recovered were 94.5 ± 5.0%.

All soil samples were weighed 0.4–0.5 g and extracted by a mixture of CuSO₄-HNO₃-CH₂Cl₂ (shaken for half an hour). The quality control for the analytical process of MeHg was carried out by using duplicates and certified reference materials (ERM-CC580 and Tort-3). The MeHg recovery for certified reference materials was 90–110% and the relative standard deviations of the duplicate samples were < 10%.

The procedures for Hg isotope measurement have been described previously^{21,50,59}. Briefly, all samples were processed by a double-stage tube furnace and trapping solutions (anti aqua regia, HNO₃:HCl = 2:1, v/v) for Hg preconcentration, and the solutions were diluted to 0.5 ng mL⁻¹ prior to Hg isotope measurement on a MC-ICP-MS (Multicollector-Inductively Coupled Plasma Mass Spectrometer, Nu-Plasma II). The acid strength of the diluted solution was about 10%. Hg standard (NIST-3133) and Hg isotope standard (NIST-8610) solutions were matched to the sample solution (0.5 ng mL⁻¹ Hg, 10% acid strength with anti-aqua regia). The Hg-MDF is reported in δ notation using the unit of permil (‰) referenced to the neighboring NIST-3133 solution:

$$\delta^{202}\text{Hg}(\text{‰}) = 1000 \times [({}^{202}\text{Hg}/{}^{198}\text{Hg})_{\text{sample}} / ({}^{202}\text{Hg}/{}^{198}\text{Hg})_{\text{NIST-3133}} - 1] \quad (3)$$

MIF is reported as Δ^{xxx}Hg following the convention suggested by Blum and Bergquist:⁶⁸

$$\Delta^{199}\text{Hg}(\text{‰}) = \delta^{199}\text{Hg} - 0.2520 \times \delta^{202}\text{Hg} \quad (4)$$

$$\Delta^{200}\text{Hg}(\text{‰}) = \delta^{200}\text{Hg} - 0.5024 \times \delta^{202}\text{Hg} \quad (5)$$

$$\Delta^{201}\text{Hg}(\text{‰}) = \delta^{201}\text{Hg} - 0.7520 \times \delta^{202}\text{Hg} \quad (6)$$

BCR-482 (vegetation SRM) and GSS-4 (soil SRM) were combusted in an oven-enrichment system after every 10 samples to assess if the non-unity recoveries resulting from the double-stage offline combustion-trapping technique induced discernible isotopic bias; their recoveries ranged from 94% to 104%. The Hg isotopic signatures of BCR-482 were measured as δ²⁰²Hg = -1.67 ± 0.12‰, Δ¹⁹⁹Hg = -0.56 ± 0.08‰, Δ²⁰⁰Hg = -0.01 ± 0.04‰ and Δ²⁰¹Hg = -0.58 ± 0.08‰ (Mean ± 2 SD, Standard deviation, n = 6), and of GSS-4 as δ²⁰²Hg = -1.72 ± 0.16‰, Δ¹⁹⁹Hg = -0.34 ± 0.06‰, Δ²⁰¹Hg = -0.34 ± 0.06‰ and Δ²⁰⁰Hg = -0.00 ± 0.04‰ (Mean ± 2 SD, n = 6). The NIST-8610 was also analyzed for every 10 samples during the Hg isotope measurements, with isotopic signatures of δ²⁰²Hg = -0.53 ± 0.08‰, Δ¹⁹⁹Hg = -0.00 ± 0.08‰ and Δ²⁰¹Hg = -0.03 ± 0.06‰ (Mean ± 2 SD, n = 12). All measured Hg isotopic signatures of these certified reference materials (CRM) were consistent with their respective recommended values^{68,69}.

Hg isotope mixing model. Δ¹⁹⁹Hg signals were utilized for estimating the contribution of root uptake soil Hg and foliage uptake atmospheric Hg⁰ in vegetation as:

$$\Delta^{199}\text{Hg}_{\text{soil}} \times f_{\text{soil-veg}} + \Delta^{199}\text{Hg}_{\text{air-Hg(0)}} \times (1 - f_{\text{soil-veg}}) = \Delta^{199}\text{Hg}_{\text{veg}} \quad (7)$$

where $f_{\text{soil-veg}}$ is the soil Hg source contribution, and Δ¹⁹⁹Hg_{air-Hg(0)} is the signature of atmospheric Hg⁰, and Δ¹⁹⁹Hg_{veg} is the signature of the vegetation foliage or root. The term “1 - $f_{\text{soil-veg}}$ ” in Eq. (7) represents the contribution from live foliage uptake atmospheric Hg⁰. Given Δ²⁰⁰Hg signatures are insensitive to Hg biogeochemical modification in the ecosystems, we estimated the Hg sources in soils as:

$$f_{\text{geo}} = (\text{Ti}/\text{Hg})_{\text{soil}} \times (\text{Hg}/\text{Ti})_{\text{crust}} \quad (8)$$

$$f_{\text{geo}} + f_{\text{soil-Hg(0)}} + f_{\text{soil-Hg(II)}} = 1 \quad (9)$$

$$\Delta^{200}\text{Hg}_{\text{geo}} \times f_{\text{geo}} + \Delta^{200}\text{Hg}_{\text{air-Hg(0)}} \times f_{\text{soil-Hg(0)}} + \Delta^{200}\text{Hg}_{\text{air-Hg(II)}} \times f_{\text{soil-Hg(II)}} = \Delta^{200}\text{Hg}_{\text{soil}} \quad (10)$$

where f_{geo} is the contribution fraction for geogenic sources (Δ²⁰⁰Hg_{geo}), and $f_{\text{soil-Hg(0)}}$ is the total contribution fraction for atmospheric Hg⁰ sources (Δ²⁰⁰Hg_{air-Hg(0)}), and $f_{\text{soil-Hg(II)}}$ is the total contribution fraction for atmospheric Hg²⁺ sources (Δ²⁰⁰Hg_{air-Hg(II)}). In addition, we also calculated root uptake of previously deposited Hg⁰ ($f_{\text{leg-Hg0}}$) in soils as:

$$f_{\text{leg-Hg0}} = f_{\text{soil-veg}} \times f_{\text{soil-Hg(0)}} \quad (11)$$

We used the intercept of Eq. (1) in the main text (-0.20 ± 0.10‰) to represent the Δ¹⁹⁹Hg_{air-Hg(0)}, which agrees with exceptional well with recently reported atmospheric Hg⁰ signatures (-0.20 ± 0.07‰) at Nyingchi, a remote site in the QTP (n = 31, Supplementary Table 3)⁴⁰. The value is also consistent with an earlier reported global average of Δ¹⁹⁹Hg for atmospheric Hg⁰ (-0.16 ± 0.11‰, n = 343)¹⁹. We note that the rhizospheric soil samples were collected from 10 cm depth root, which may not represent the entire soil matrix from where root uptake of Hg takes place. Hence, we used the average Δ¹⁹⁹Hg value of 0–17 cm soils and rhizospheric soils to represent the Δ¹⁹⁹Hg_{soil} at each site.

The Δ²⁰⁰Hg signatures are caused by photo-oxidation in the troposphere and relatively insensitive to other Hg biogeochemical processes^{36,39}, thus can be used as a powerful tracer to identify Hg sources that are atmospheric in origin. Using the Hg/Ti ratios and Δ²⁰⁰Hg signatures, we are able to quantify the contributions from

various sources to Hg in the uppermost soil profiles. The average of $\Delta^{200}\text{Hg}$ in rainfall across the QTP is $0.19 \pm 0.05\text{‰}$ (Supplementary Table 1) and the atmospheric Hg^0 in the global remote regions has an average value of $-0.05 \pm 0.05\text{‰}$ ^{19,70}. Both mean values are used in our modeling.

Since the Hg isotopic signature of the soil solution is unknown, uncertainty exists in estimating the contribution of atmospheric Hg^{2+} sources in the isotopic mixing models. There is also a knowledge gap in the measurement of gaseous oxidized Hg^{71-73} , resulting in analytical uncertainty of the reported MIF signatures. The oxidation of Hg^0 in the tropopause is suggested as the main cause for the $\Delta^{200}\text{Hg}$ signature in precipitation³⁹. The stratospheric intrusion in the QTP may lead to the enrichment of atmospheric Hg^{2+} concentrations at higher elevations^{74,75}. We assumed constant $\Delta^{199}\text{Hg}$ and $\Delta^{200}\text{Hg}$ values in atmospheric Hg inputs without considering elevational differences. Our earlier studies have suggested the Hg isotope mixing models associated with Monte Carlo simulations could reduce the uncertainties of the model results^{20,21}. These uncertainties are quantified by generating one million groups of MIF signatures randomly ranging from Mean-2SD to Mean + 2 SD to solve the Hg isotope mixing models. Given at the 95% confidence level, our models' uncertainty ranges between 16% and 40% (2 SD, details in Supplementary Fig. 9–15).

Statistical methods. Data were analyzed by using the statistical program R 4.10 and SPSS 26.0 with $p < 0.05$ as the level of statistical significance. We used the generalized linear model (GLM) to analyze the spatial response among values of Hg concentration, pool size, isotopic signatures, altitude and precipitation. GLM is a generalization of ordinary linear regression that allows for response variables that have error distribution models other than a normal distribution like the Gaussian distribution. In addition, we used Independent Samples T-test, One-Way ANOVA and post hoc Tukey HSD to conduct the significant difference analysis when data were normally distributed; otherwise, we used the Kruskal-Wallis test.

Reporting summary. Further information on research design is available in the Nature Portfolio Reporting Summary linked to this article.

Data availability

Data of precipitation in the TGR are obtained from National Tibetan Plateau/Third Pole Environment Data Center (<https://data.tpdc.ac.cn/en/data/3fc66dcd-5db9-4af4-bf6c-55671875a400/>). The permafrost distribution on the Tibetan Plateau is from the earlier study (<https://doi.org/10.5194/tc-11-2527-2017>). The Supplementary Data for Figs. 1–5 can be found in Supplementary Data 1–5 and TPDC repository (<https://data.tpdc.ac.cn/en/data/710c7822-ed71-47d4-831f-6c0365de6dcb/>). Code sharing not applicable to this article as no custom codes or mathematical algorithms that is deemed central to the conclusions.

Received: 25 March 2022; Accepted: 8 November 2022;

Published online: 19 November 2022

References

- Selin, H. et al. Linking science and policy to support the implementation of the Minamata Convention on Mercury. *Ambio* **47**, 198–215 (2018).
- UN-Environment. Global Mercury Assessment 2018. UN-Environment Programme, Chemicals and Health Branch (2019).
- Outridge, P. M., Mason, R. P., Wang, F., Guerrero, S. & Heimburger-Boavida, L. E. Updated global and oceanic mercury budgets for the United Nations Global Mercury Assessment 2018. *Environ. Sci. Technol.* **52**, 11466–11477 (2018).
- Wang, F. et al. How closely do mercury trends in fish and other aquatic wildlife track those in the atmosphere?—Implications for evaluating the effectiveness of the Minamata convention. *Sci. Total Environ.* **674**, 58–70 (2019).
- Lim, A. G. et al. A revised pan-Arctic permafrost soil Hg pool based on Western Siberian peat Hg and carbon observations. *Biogeosciences* **17**, 3083–3097 (2020).
- Schuster, P. F. et al. Permafrost stores a globally significant amount of mercury. *Geophys. Res. Lett.* **45**, 1463–1471 (2018).
- Ci, Z., Peng, F., Xue, X. & Zhang, X. Permafrost thaw dominates mercury emission in Tibetan thermokarst Ponds. *Environ. Sci. Technol.* **54**, 5456–5466 (2020).
- Mu, C. et al. Permafrost degradation enhances the risk of mercury release on Qinghai-Tibetan Plateau. *Sci. Total Environ.* **708**, 135127 (2020).
- Schaefer, K. et al. Potential impacts of mercury released from thawing permafrost. *Nat. Commun.* **11**, 4650 (2020).
- Obrist, D. et al. Tundra uptake of atmospheric elemental mercury drives Arctic mercury pollution. *Nature* **547**, 201–204 (2017).
- Olson, C. L., Jiskra, M., Sonke, J. E. & Obrist, D. Mercury in tundra vegetation of Alaska: spatial and temporal dynamics and stable isotope patterns. *Sci. Total Environ.* **660**, 1502–1512 (2019).
- Ding, J. Z. et al. Decadal soil carbon accumulation across Tibetan permafrost regions. *Nat. Geosci.* **10**, 420–424 (2017).
- Bockheim, J. G. & Munroe, J. S. Organic carbon pools and genesis of Alpine soils with permafrost: a review. *Arctic, Antarct., Alp. Res.* **46**, 987–1006 (2018).
- Wei, D. et al. Plant uptake of CO₂ outpaces losses from permafrost and plant respiration on the Tibetan Plateau. *Proc. Natl Acad. Sci. USA* **118**, e2015283118 (2021).
- Ci, Z., Peng, F., Xue, X. & Zhang, X. Air-surface exchange of gaseous mercury over permafrost soil: an investigation at a high-altitude (4700 m a.s.l.) and remote site in the central Qinghai-Tibet Plateau. *Atmos. Chem. Phys.* **16**, 14741–14754 (2016).
- Leonard, T. L., Taylor, G. E., Gustin, M. S. & Fernandez, G. C. J. Mercury and plants in contaminated soils: 1. Uptake, partitioning, and emission to the atmosphere. *Environ. Toxicol. Chem.* **17**, 2063–2071 (1998).
- Lindberg, S. E. et al. Atmospheric emission and plant uptake of mercury from agricultural soils near the almaden mercury mine. *J Environ. Qual.* **8**, 572–578 (1979).
- Bishop, K. H., Lee, Y. H., Munthe, J. & Dambrine, E. Xylem sap as a pathway for total mercury and methylmercury transport from soils to tree canopy in the boreal forest. *Biogeochemistry* **40**, 101–113 (1998).
- Wang, X., Yuan, W., Lin, C.-J. & Feng, X. Mercury cycling and isotopic fractionation in global forests. *Crit. Rev. Environ. Sci. Technol.* **52**, 3763–3786 (2021).
- Wang, X. et al. Global warming accelerates uptake of atmospheric mercury in regions experiencing glacier retreat. *Proc. Natl Acad. Sci. USA* **117**, 2049–2055 (2020).
- Wang, X. et al. Underestimated sink of atmospheric mercury in a deglaciated forest chronosequence. *Environ. Sci. Technol.* **54**, 8083–8093 (2020).
- Wang, X. et al. Climate and vegetation as primary drivers for global mercury storage in surface soil. *Environ. Sci. Technol.* **53**, 10665–10675 (2019).
- Jiskra, M. et al. Mercury deposition and re-emission pathways in boreal forest soils investigated with Hg isotope signatures. *Environ. Sci. Technol.* **49**, 7188–7196 (2015).
- Demers, J. D., Blum, J. D. & Zak, D. R. Mercury isotopes in a forested ecosystem: Implications for air-surface exchange dynamics and the global mercury cycle. *Glob. Biogeochem. Cycles* **27**, 222–238 (2013).
- Meng, B. et al. Tracing the uptake, transport, and fate of Mercury in Sawgrass (*Cladium jamaicense*) in the Florida everglades using a multi-isotope technique. *Environ. Sci. Technol.* **52**, 3384–3391 (2018).
- Mao, Y., Li, Y., Richards, J. & Cai, Y. Investigating Uptake and Translocation of Mercury Species by Sawgrass (*Cladium jamaicense*) Using a Stable Isotope Tracer Technique. *Environ. Sci. Technol.* **47**, 9678–9684 (2013).
- Wang, J. J. et al. Fine root mercury heterogeneity: metabolism of lower-order roots as an effective route for mercury removal. *Environ. Sci. Technol.* **46**, 769–777 (2012).
- Cui, L. W. et al. Accumulation and translocation of (198)Hg in four crop species. *Environ. Toxicol. Chem.* **33**, 334–340 (2014).
- Gao, Z. et al. Root-induced changes to soil water retention in permafrost regions of the Qinghai-Tibet Plateau, China. *J. Soil Sediment.* **18**, 791–803 (2017).
- Blume-Werry, G., Milbau, A., Teuber, L. M., Johansson, M. & Dorrepaal, E. Dwelling in the deep—strongly increased root growth and rooting depth enhance plant interactions with thawing permafrost soil. *N. Phytol.* **223**, 1328–1339 (2019).
- Motta, L. C., Chien, A. D., Rask, A. E. & Zimmerman, P. M. Mercury/magnetic isotope effect: a plausible photochemical mechanism. *J Phys. Chem. A* **124**, 3711–3719 (2020).
- Motta, L. C., Kritee, K., Blum, J. D., Tsz-Ki Tsui, M. & Reinfelder, J. R. Mercury isotope fractionation during the photochemical reduction of Hg(II) coordinated with organic ligands. *J. Phys. Chem. A* **124**, 2842–2853 (2020).
- Zheng, W. & Hintelmann, H. Isotope fractionation of mercury during its photochemical reduction by low-molecular-weight organic compounds. *J. Phys. Chem. A* **114**, 4246–4253 (2010).
- Kalbitz, K., Solinger, S., Park, J. H., Michalzik, B. & Matzner, E. Controls on the dynamics of dissolved organic matter in soils: a review. *Soil Sci.* **165**, 277–304 (2000).
- Yin, A. & Harrison, T. M. Geologic evolution of the Himalayan-Tibetan orogen. *Annu. Rev. Earth Planet. Sci.* **28**, 211–280 (2000).
- Blum, J. D., Sherman, L. S. & Johnson, M. W. Mercury isotopes in earth and environmental sciences. *Annu. Rev. Earth Planet. Sci.* **42**, 249–269 (2014).
- Yu, B. et al. Isotopic composition of atmospheric mercury in China: new evidence for sources and transformation processes in air and in vegetation. *Environ. Sci. Technol.* **50**, 9262–9269 (2016).

38. Sun, R. et al. Modelling the mercury stable isotope distribution of Earth surface reservoirs: implications for global Hg cycling. *Geochim. Cosmochim. Acta.* **246**, 156–173 (2019).
39. Chen, J. B., Hintelmann, H., Feng, X. B. & Dimock, B. Unusual fractionation of both odd and even mercury isotopes in precipitation from Peterborough, ON, Canada. *Geochim. Cosmochim. Acta.* **90**, 33–46 (2012).
40. Yu, B. et al. Tracing the transboundary transport of mercury to the Tibetan plateau using atmospheric mercury isotopes. *Environ. Sci. Technol.* **56**, 1568–1577 (2022).
41. Diaz, O. et al. Total and bioavailable arsenic concentration in arid soils and its uptake by native plants from the pre-Andean zones in Chile. *Bull. Environ. Contam. Toxicol.* **86**, 666–669 (2011).
42. Burghelca, C. et al. Mineral nutrient mobilization by plants from rock: influence of rock type and arbuscular mycorrhiza. *Biogeochemistry* **124**, 187–203 (2015).
43. Lyu, S. et al. Titanium as a beneficial element for crop production. *Front. Plant Sci.* **8**, 597 (2017).
44. Wu, W. J., Zhou, G. S. & Xu, Z. Z. Driving mechanisms of climate-plant-soil patterns on the structure and function of different grasslands along environmental gradients in Tibetan and Inner Mongolian Plateaus in China. *J. Clean. Prod.* **339**, 130696 (2022).
45. Wang, X. et al. Genomic basis of high-altitude adaptation in Tibetan Prunus fruit trees. *Curr. Biol.* **31**, 3848–3860.e3848 (2021).
46. Abbas, M. et al. An oxygen-sensing mechanism for angiosperm adaptation to altitude. *Nature* **606**, 565–569 (2022).
47. Wu, J.-S., Shen, Z.-X., Zhang, X.-Z. & Shi, P.-L. Biomass allocation patterns of alpine grassland species and functional groups along a precipitation gradient on the Northern Tibetan Plateau. *J. Mt. Sci.* **10**, 1097–1108 (2013).
48. Yuan, W. et al. Stable isotope evidence shows re-emission of elemental mercury vapor occurring after reductive loss from foliage. *Environ. Sci. Technol.* **53**, 651–660 (2019).
49. Zhou, J., Obrist, D., Dastoor, A., Jiskra, M. & Ryjkov, A. Vegetation uptake of mercury and impacts on global cycling. *Nat. Rev. Earth Environ.* **2**, 269–284 (2021).
50. Wang, X. et al. Using mercury isotopes to understand mercury accumulation in the montane forest floor of the eastern Tibetan Plateau. *Environ. Sci. Technol.* **51**, 801–809 (2017).
51. Yuan, W. et al. Quantification of atmospheric mercury deposition to and legacy re-emission from a subtropical forest floor by mercury isotopes. *Environ. Sci. Technol.* **55**, 12352–12361 (2021).
52. Zhang, H. et al. Atmospheric mercury inputs in montane soils increase with elevation: evidence from mercury isotope signatures. *Sci. Rep.* **3**, 3322 (2013).
53. Zheng, W. & Hintelmann, H. Nuclear field shift effect in isotope fractionation of mercury during abiotic reduction in the absence of light. *J. Phys. Chem. A* **114**, 4238–4245 (2010).
54. Zheng, W. et al. Mercury stable isotope fractionation during abiotic dark oxidation in the presence of thiols and natural organic matter. *Environ. Sci. Technol.* **53**, 1853–1862 (2019).
55. Tsui, M. T., Blum, J. D. & Kwon, S. Y. Review of stable mercury isotopes in ecology and biogeochemistry. *Sci. Total Environ.* **716**, 135386 (2020).
56. Ci, Z., Peng, F., Xue, X. & Zhang, X. Temperature sensitivity of gaseous elemental mercury in the active layer of the Qinghai-Tibet Plateau permafrost. *Environ. Pollut.* **238**, 508–515 (2018).
57. Sun, S. et al. Vegetation mediated mercury flux and atmospheric mercury in the Alpine permafrost region of the Central Tibetan Plateau. *Environ. Sci. Technol.* **54**, 6043–6052 (2020).
58. Olson, C., Jiskra, M., Biester, H., Chow, J. & Obrist, D. Mercury in active-layer tundra soils of Alaska: concentrations, pools, origins, and spatial distribution. *Glob. Biogeochem. Cycles* **32**, 1058–1073 (2018).
59. Wang, X., Yuan, W., Feng, X., Wang, D. & Luo, J. Moss facilitating mercury, lead and cadmium enhanced accumulation in organic soils over glacial erratic at Mt. Gongga, China. *Environ. Pollut.* **254**, 112974 (2019).
60. Wang, P. et al. Belowground plant biomass allocation in tundra ecosystems and its relationship with temperature. *Environ. Res. Lett.* **11**, 055003 (2016).
61. Yang, Y. H., Fang, J. Y., Ji, C. J. & Han, W. X. Above- and belowground biomass allocation in Tibetan grasslands. *J. Veg. Sci.* **20**, 177–184 (2009).
62. Mu, C. et al. Impacts of permafrost on above- and belowground biomass on the northern Qinghai-Tibetan Plateau. *Arct. Antarct. Alp. Res.* **50**, e1447192 (2018).
63. Gu, J. et al. The driving factors of mercury storage in the Tibetan grassland soils underlain by permafrost. *Environ. Pollut.* **265**, 115079 (2020).
64. Sun, R. et al. Mercury biogeochemistry over the Tibetan Plateau: an overview. *Crit. Rev. Environ. Sci. Technol.* **51**, 577–602 (2020).
65. Sheng, J., Wang, X., Gong, P., Tian, L. & Yao, T. Heavy metals of the Tibetan top soils: level, source, spatial distribution, temporal variation and risk assessment. *Environ. Sci. Pollut. Res. Int.* **19**, 3362–3370 (2012).
66. Wang, X., Yuan, W., Lin, C. J., Wu, F. & Feng, X. Stable mercury isotopes stored in Masson Pinus tree rings as atmospheric mercury archives. *J. Hazard. Mater.* **415**, 125678 (2021).
67. Walkley A. A critical examination of a rapid method for determining organic carbon in soils—effect of variations in digestion conditions and of inorganic soil constituents. *Soil Sci.* **63**, (1947).
68. Blum, J. D. & Bergquist, B. A. Reporting of variations in the natural isotopic composition of mercury. *Anal. Bioanal. Chem.* **388**, 353–359 (2007).
69. Estrade, N., Carignan, J., Sonke, J. E. & Donard, O. F. X. Measuring Hg isotopes in bio-geo-environmental reference materials. *Geostand. Geoanal. Res.* **34**, 79–93 (2010).
70. Jiskra, M. et al. Mercury stable isotopes constrain atmospheric sources to the ocean. *Nature* **597**, 678–682 (2021).
71. Gustin, M. S., Amos, H. M., Huang, J., Miller, M. B. & Heidecorn, K. Measuring and modeling mercury in the atmosphere: a critical review. *Atmos. Chem. Phys.* **15**, 5697–5713 (2015).
72. Huang, J. Y. & Gustin, M. S. Uncertainties of gaseous oxidized mercury measurements using KCl-coated denuders, cation-exchange membranes, and nylon membranes: humidity influences. *Environ. Sci. Technol.* **49**, 6102–6108 (2015).
73. Fu, X. et al. Mass-independent fractionation of even and odd mercury isotopes during atmospheric mercury redox reactions. *Environ. Sci. Technol.* **55**, 10164–10174 (2021).
74. Zhang, H., Fu, X. W., Lin, C. J., Wang, X. & Feng, X. B. Observation and analysis of speciated atmospheric mercury in Shangri-La, Tibetan Plateau, China. *Atmos. Chem. Phys.* **15**, 653–665 (2015).
75. Fu, X. W. et al. Temporal trend and sources of speciated atmospheric mercury at Waliguan GAW station, Northwestern China. *Atmos. Chem. Phys.* **12**, 1951–1964 (2012).
76. Zou, D. et al. A new map of permafrost distribution on the Tibetan Plateau. *Cryosphere* **11**, 2527–2542 (2017).

Acknowledgements

This work was funded by National Natural Science Foundation of China (42122053), Strategic Priority Research Programs of the Chinese Academy of Sciences, the Pan-Third Pole Environment Study for a Green Silk Road (Pan-TPE, XDA2004050201), and Second Tibetan Plateau Scientific Expedition and Research Program (STEP, No.2019QZKK0307). Thank Mr. Xianming Li, Nantao Liu, Ge Zhang, and Fei Wu for the help of sample measurements.

Author contributions

X.W. and X.B.F. designed the research; X.W., J.C.X., J.L. W.Z., D.Y.W., and Y.W. performed research; X.W. and Y.W. analyzed data; X.W. drafted the manuscript; C.J.L., F.Y.W., and X.B.F. reviewed and revised the paper.

Competing interests

The authors declare no competing interests.

Additional information

Supplementary information The online version contains supplementary material available at <https://doi.org/10.1038/s43247-022-00619-y>.

Correspondence and requests for materials should be addressed to Xinbin Feng.

Peer review information *Communications Earth & Environment* thanks the anonymous reviewers for their contribution to the peer review of this work. Primary Handling Editors: Erika Buscardo and Clare Davis.

Reprints and permission information is available at <http://www.nature.com/reprints>

Publisher's note Springer Nature remains neutral with regard to jurisdictional claims in published maps and institutional affiliations.



Open Access This article is licensed under a Creative Commons Attribution 4.0 International License, which permits use, sharing, adaptation, distribution and reproduction in any medium or format, as long as you give appropriate credit to the original author(s) and the source, provide a link to the Creative Commons license, and indicate if changes were made. The images or other third party material in this article are included in the article's Creative Commons license, unless indicated otherwise in a credit line to the material. If material is not included in the article's Creative Commons license and your intended use is not permitted by statutory regulation or exceeds the permitted use, you will need to obtain permission directly from the copyright holder. To view a copy of this license, visit <http://creativecommons.org/licenses/by/4.0/>.

© The Author(s) 2022